Solar Physics (2005) 227: 231–248 

# UPDATED EXPRESSIONS FOR DETERMINING TEMPERATURES AND EMISSION MEASURES FROM GOES SOFT X-RAY MEASUREMENTS

STEPHEN M. WHITE[1], ROGER J. THOMAS[2] and RICHARD A. SCHWARTZ[2]
[1]*Department of Astronomy, University of Maryland, College Park, MD 20742, U.S.A.*
[2]*Code 682, NASA/Goddard Space Flight Center, Greenbelt, MD 20771, U.S.A.*
*(e-mail: white@astro.umd.edu)*

(Received 14 December 2004; accepted 12 February 2005)

**Abstract.** We investigate the conversion of the 0.5–4 and 1–8 Å soft X-ray flux measurements made by detectors on the Geostationary Operational Environmental Satellites (GOES) into temperature and emission measures of coronal plasma using modern spectral models and modern understanding of coronal abundances. In particular, the original analysis by Thomas, Starr and Crannell (1985) is updated to take into account the realization that coronal abundances may be quite different from photospheric abundances. An important result of this analysis is that the derived temperatures and emission measures depend strongly on the assumed abundances even at high temperatures where continuum rather than spectral lines dominates the Sun's X-ray spectrum. This occurs because the higher coronal abundances mean that most of the continuum is due to free–bound emission processes, not free–free emission, and thus is abundance-dependent. We find significant differences between modern calculations of the temperature response of the flux measurements and the versions currently in use: for a typical flare, emission measures may be up to a factor of 4 smaller than the current software suggests. Derived temperatures are similar for both photospheric and coronal abundances for cool flares (e.g., 15 MK), but for hot flares (e.g., 35 MK) coronal abundances can lead to significantly (∼25%) lower temperatures being derived.

## 1. Introduction

The National Oceanic and Atmospheric Administration (NOAA) launches and maintains a set of satellites called Geostationary Operational Environmental Satellites (GOES), carrying weather monitoring instruments. Each GOES satellite also carries a solar X-ray package (the "X-Ray Sensor", or XRS) consisting of a collimator that feeds a pair of ion chambers. These ion chambers measure the Sun's spatially integrated soft X-ray flux in two wavelength bands, 0.5–4 and 1–8 Å, with a 3-s cadence. The GOES soft X-ray detectors have provided an essentially uninterrupted monitor of the Sun's activity for 30 years, and are a valuable resource for the study of past solar activity and the prediction of space weather (e.g., Bornmann, 1990; Phillips and Feldman, 1995; Aschwanden and Alexander, 2001; Garcia, 2004).

For quantitative physical understanding of processes in the Sun's atmosphere, the X-ray fluxes themselves are of limited use. However, they reflect the temperature and emission measure of the plasma that produces the soft X-rays, and these physical

quantities are of great importance: from them, the energetics of solar flares and other energy releases can be deduced, and their time variations can be interpreted directly in terms of physical models (e.g., Veronig *et al.*, 2005). They can also be used for comparison with radio fluxes due to thermal bremsstrahlung. In order to use the GOES soft X-ray fluxes for such studies, Thomas, Starr, and Crannell (1985, abbreviated as TSC) investigated the response of the two soft X-ray bands as a function of the temperature of the radiating plasma and showed that the temperature and emission measure of hot plasma ($\sim$10 MK) can be derived in a straightforward fashion under the isothermal assumption: the ratio of the fluxes in the two GOES XRS bands unambiguously determines the (model-dependent) temperature, and once this is known the X-ray flux in one of the bands determines the (model-dependent) emission measure.

TSC determined the temperature response by folding model X-ray spectra of isothermal plasmas through the response of the GOES 1 XRS detectors and produced handy polynomial approximations that have been widely used to derive temperatures and emission measures from GOES fluxes. These quantities are volume-averaged, since they have no spatial resolution, but, e.g., during flares the flare emission can easily be isolated by background subtraction and the quantities so derived are physically representative. Since they are obtained from just two numbers, they cannot accommodate the widely recognized multi-thermal nature of the solar corona, i.e., the fact that at any given time the corona is inhomogeneous and different temperature plasmas are present at different locations. However, for topics such as overall energetics, the volume-averaged quantities represented by the GOES XRS data remain important tools.

The motivation to revisit the determination of temperature and emission measure from GOES XRS data comes from two notable developments. The first is improvements in modeling of solar X-ray spectra that have taken place. Spectra in the relevant temperature range (roughly 5–30 MK) contain both continuum and spectral lines, and depend on the ionization equilibrium of each atomic species as well as the transition strengths of the lines. Both these topics are much better understood than was the case in 1985. Secondly, and probably more importantly, is the recognition that the abundance distribution in the solar corona need not be the same as in the solar photosphere. At about the time of the TSC analysis it was starting to be recognized that abundance distributions actually depend on the amount of energy required to remove the outermost electron from an element's neutral atom. This so-called "FIP-effect" (for first ionization potential) results in low-FIP elements, such as Fe, having a higher abundance in the corona relative to high-FIP elements, such as O, than they do in the photosphere (Meyer, 1985). Because of the difficulty of measuring absolute abundances, debate as to whether low-FIP elements were enhanced in the corona or high-FIP elements were depleted in the corona (relative to the photosphere) continued for some time. However, a consensus seems to have emerged that high-FIP elements have the same absolute abundance in the corona as in the photosphere, while the low-FIP elements are enhanced in the corona by a

factor of order 4 (Feldman, 1992; Feldman and Laming, 2000; White *et al.*, 2000). The picture is complicated by evidence that the enhancement factor is not steady, but varies with time and location and may depend, for example, on the age of an active region (Fludra and Schmelz, 1999; Schmelz, 1999; Feldman and Widing, 2003).

There have been other analyses of the GOES XRS data since TSC. Garcia (1994) describes the operation of the GOES XRS detectors in great detail, and particularly the differences between satellites. He used spectra calculated with both the Raymond (Raymond and Smith, 1977) and Mewe (Mewe, Gronenschild, and van den Oord, 1985) models to determine the temperature response. The nature of the abundances and ionization equilibrium used is not described. Sylwester, Garcia, and Sylwester (1995) extend Garcia's analysis, but also did not investigate the role of abundances. R. A. Schwartz implemented the differences between detectors on different satellites discussed in these papers in the `goes` routine in the SolarSoft package (Freeland and Handy, 1998), and used model spectra from the SolarSoft task `mewe_spec`, which is based on the Mewe model with Meyer coronal abundances (Meyer, 1985), to determine the temperature response of the GOES XRS detectors.

In this paper we repeat the analysis of TSC, Garcia (1994) and Sylwester, Garcia, and Sylwester (1995) using modern model spectra from the CHIANTI database (Dere *et al.*, 1997; Young, Landi, and Thomas, 1998), and compare the results for both coronal and photospheric abundances with the earlier work, and with the GOES analysis software that has been available in the SolarSoft package. We find significant differences, primarily resulting from the abundance issue. However, it may be surprising that the main effect is not in the spectral lines, but rather in the free–bound contribution to the continuum emission. This can be larger than the free–free emission in the relevant temperature range, and therefore the effect is still important at higher temperatures where the spectral lines are less significant.

## 2. GOES XRS Transfer Functions

The detailed nature of the response of the GOES XRS detectors to soft X-rays is described by TSC and Garcia (1994). The raw measured quantities are currents induced in the ion chambers by the incident X-rays. The detectors are calibrated prior to launch. The "transfer functions" that represent the measured response (detector current per incident X-ray flux) as a function of wavelength are shown in Figure 1 for GOES 1–12 (these are the functions used in the GOES software routines in SolarSoft). The point of this figure is that there are differences between detectors on the different satellites, but they are relatively small.

The actual X-ray fluxes incident on the detectors are not known, since different spectral forms can produce the same currents. The reported X-ray fluxes are derived

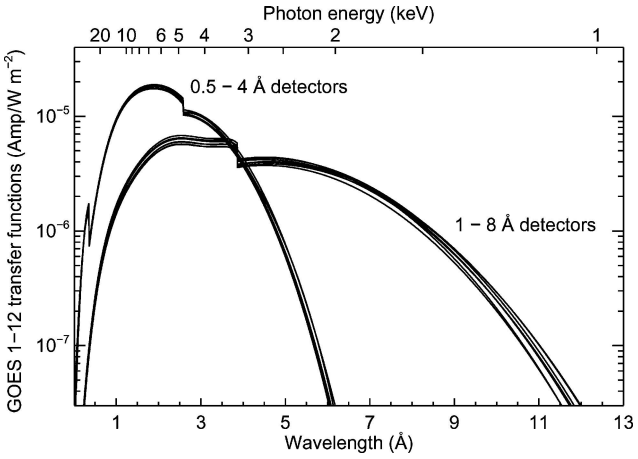


*Figure 1.* The "transfer functions" G(λ) for the 0.5–4 and 1–8 Å XRS detectors on GOES satellites 1–12, overplotted without distinction. This plot indicates the variation in the response of the detectors on the different satellites.

by assuming that a wavelength-averaged response is appropriate for each detector. The coefficients used to convert the currents measured in the ion chambers into the reported X-ray fluxes can differ significantly from one satellite to the next. These coefficients, labeled $\bar{G}_4$ (0.5–4 Å channel) and $\bar{G}_8$ (1–8 Å channel), are tabulated in the appendix (we thank Rodney Viereck of NOAA for supplying the previously unavailable calibration data for the XRS detectors on the GOES 12 satellite). They represent wavelength-averaged transfer functions (see Garcia, 1994, and TSC), in units of A/(W m$^{-2}$).

$\bar{G}_4$ varies by up to 40% from early satellites to later versions, mostly due to a decision to normalize the shorter-wavelength channel over the range 0.5–3 Å rather than 0.5–4 Å (discussed by Garcia, 1994), while $\bar{G}_8$ can differ by 20%. The different values of the $\bar{G}$ coefficients affect the temperature response in terms of the X-ray fluxes. This is discussed in the next section. However, we emphasize that it is only the derived temperatures and emission measures that depend on the models used to represent X-ray spectra from hot plasma, not the actual currents in the ion chambers themselves.

## 3. Spectral Models

To determine the temperature response of the reported GOES XRS fluxes, we convolve the wavelength–dependent transfer functions in Figure 1 with models of the X-ray spectrum of an isothermal plasma and convert them to GOES X-ray fluxes using the formalism described by TSC and Garcia, (1994) with $\bar{G}$ coefficients from Table I. We use models calculated using version 4.2 of the CHIANTI

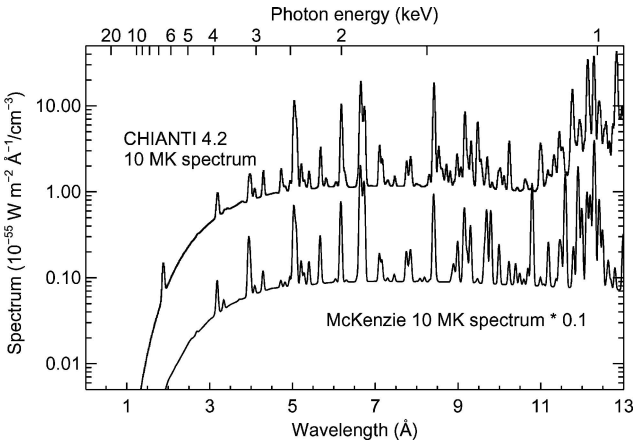


*Figure 2.* A comparison of the model spectrum for a 10 MK plasma obtained from CHIANTI 4.2 with photospheric abundances (*upper curve*) with the 10 MK spectrum calculated by McKenzie (*lower curve*) and used by TSC in their original calculations of the GOES XRS temperature response. The McKenzie spectrum has been divided by 10 to offset it from the CHIANTI spectrum. The spectral resolution is 0.05 Å. The wavelength scale is shown on the bottom axis and the corresponding photon energy scale on the top axis.

package[1] (Landi *et al.*, 1999; Landi, Feldman, and Dere, 2002). Ionization equilibrium is determined using the Mazzotta *et al.* (1998) calculations as implemented in CHIANTI. Continuum from free–free, free–bound and two-photon processes is included (Landi *et al.*, 1999). Spectra from 0.01 to 20 Å were calculated with 0.01 Å wavelength bins for 41 temperatures logarithmically spaced from 1.0 to 100.0 MK using both the solar coronal abundances and the solar photospheric abundances incorporated in CHIANTI. A density of $10^{10}$ cm$^{-3}$ was assumed for the calculations; we compared spectra at 10 MK for densities of $10^{9}$ cm$^{-3}$, $10^{10}$ cm$^{-3}$ and $10^{11}$ cm$^{-3}$, and found no significant differences between them, so our results should be essentially independent of the assumed density, at least over that range.

To illustrate developments in spectral modeling since the TSC work, in Figure 2 we compare the CHIANTI 4.2 spectrum at 10 MK with the spectrum used by TSC at 10 MK. For their temperature-dependence calculations, TSC used spectra provided by McKenzie based on calculations by Walker (see Walker, Jr., Rugge, and Weiss, 1974) with other supporting material, and used ionization-balance calculations by Jordan (1970). These spectra do not show all the lines found in modern CHIANTI spectra, but most of the strong lines are present and the continuum has the same shape. An obvious difference between the older McKenzie spectrum and

[1]CHIANTI 5.0 is due to be released in early 2005 and includes some additional lines in the 8–11 Å region not present in 4.2. We have compared a CHIANTI 5.0 spectrum for a 10 MK plasma supplied by Enrico Landi with the CHIANTI 4.2 spectrum used here and find that it produces a GOES XRS response that differs by of order 5% from our results. The CHIANTI 5.0 models will be used in the SolarSoft analysis software once they become available.

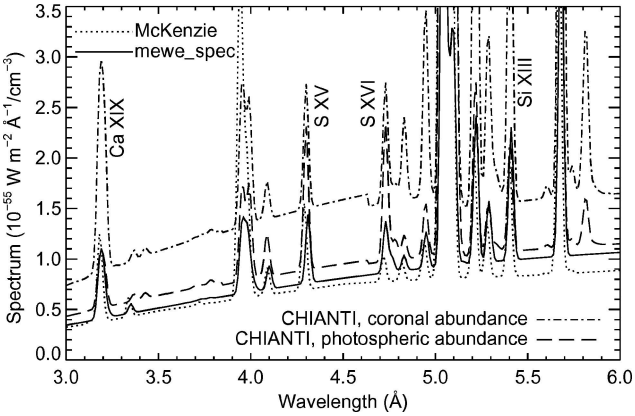


*Figure 3.* Comparison in the 3–6 Å range of model spectra at 10 MK: the CHIANTI 4.2 spectrum with coronal abundances (*dot-dashed line*), the CHIANTI 4.2 spectrum with photospheric abundances (*long-dashed line*), the `mewe_spec` spectrum presently used in the SolarSoft `goes` task (*solid line*), and the McKenzie spectrum used by TSC (*dotted line*). The spectral resolution is 0.03 Å in all spectra. Four individual lines are labeled: low-FIP Ca and Si lines, and high-FIP S lines. In this figure, the vertical scale is linear and all spectra are plotted on the same scale.

the modern spectrum is in the forest of Fe L-shell lines that form almost a bright quasi-continuum from 12–15 Å in the CHIANTI spectrum (Liedahl, Osterheld, and Goldstein, 1995; Savin *et al.*, 1996; Gu *et al.*, 2001; Brown *et al.*, 2002), where the McKenzie spectrum is much weaker. However, these lines are outside the main wavelength sensitivity of the GOES XRS 1–8 Å channel (Figure 1) and so this difference does not affect significantly the quantities derived from the GOES XRS fluxes.

To compare the continuum and the effects of the assumed abundances in more detail, Figure 3 shows the coronal and photospheric abundance CHIANTI 10 MK spectra and the McKenzie 10 MK spectrum in the 3–6 Å range. The continuum in the coronal abundance CHIANTI spectrum is considerably higher than in the photospheric abundance CHIANTI spectrum, which in turn is about 10% higher than in the McKenzie spectrum. Inspection of the lines that are common to all three spectra indicates that the McKenzie spectra were probably calculated with abundances close to solar photospheric values, which is what we would expect for that epoch. We also compared these spectra with the results of the `mewe_spec` code in SolarSoft, which uses the Mewe models and assumes "Meyer coronal" abundances (Meyer, 1985) in which the low-FIP lines are at solar photospheric values and high-FIP lines are depressed relative to their photospheric abundances. This spectrum has a continuum level very similar to the photospheric abundance CHIANTI spectrum (as it should since the CHIANTI continuum calculation is based on the Mewe calculation) and, as expected, high-FIP lines (demonstrated by the labeled S lines) that are weaker than their counterparts in the CHIANTI photospheric-abundance

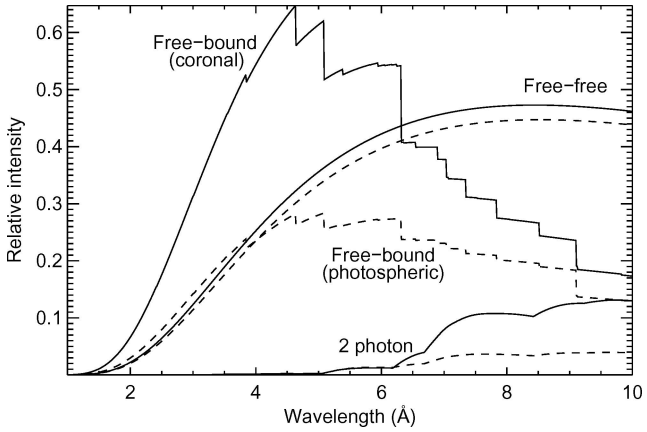


*Figure 4.* Comparison of the three contributions to the continuum level in CHIANTI 4.2 isothermal spectra at 10 MK. The free–bound, free–free and two-photon continua for coronal abundances (*solid lines*) and photospheric abundances (*dashed lines*) are labeled. The curves are normalized to the peak intensity of the total coronal-abundance continuum emission (the sum of the three solid-line curves plotted). The sharp edges in the free–bound continuum spectra represent transitions to different charge states of common ions.

and coronal-abundance spectra. By contrast, the low-FIP Ca and Si lines have similar strength in the CHIANTI photospheric-abundance and `mewe_spec` spectra, but are much stronger in the CHIANTI coronal-abundance spectrum.

The reason for the much higher continuum level in the coronal-abundance spectrum is the dominance of free–bound emission in this wavelength range. Figure 4 shows the relative contributions of free–bound, free–free and two-photon continua for coronal and photospheric abundances at 10 MK (see also Figure 6 of Young *et al.* (2003), which is the same plot but for the photospheric abundance case only). The free–bound emission depends on the higher-Z elements and therefore is abundance-dependent: for coronal abundances, the free–bound emission at this temperature is about twice the free–free emission below 6 Å. Just as importantly, because the free–bound continuum peaks at shorter wavelengths, it pushes the peak of the total continuum emission to shorter wavelengths at temperatures above 10 MK. This increases the flux in the 0.5–4 Å channel relative to the 1–8 Å channel for the same temperature, and thus in some temperature ranges (above 15 MK) the ratio of the flux in the 0.5–4 Å channel ($B_4$) to the flux in the 1–8 Å channel ($B_8$) will be larger for a given temperature if the emitting plasma has coronal rather than photospheric abundances (see also Figure 7). Note that if one replots Figure 4 for other temperatures one finds that as temperature increases the free–free continuum emission increases faster than the free–bound, so that for coronal abundances the two contributions to the continuum are roughly equal at 20 MK.

It is sometimes assumed that at high temperatures the abundance issue is irrelevant for the conversion of GOES XRS fluxes to temperature and emission measure

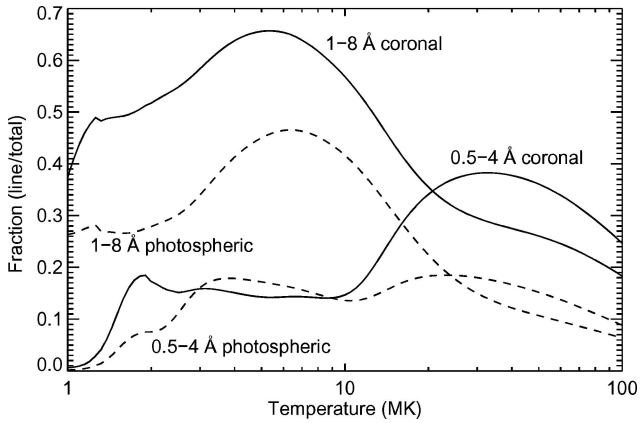


*Figure 5.* The relative contribution of spectral lines to the reported X-ray fluxes in the two GOES XRS channels as a function of temperature for coronal abundances (*solid curves*) and photospheric abundances (*dotted curves*). This calculation was carried out for the GOES 10 responses using spectra from CHIANTI 4.2.

because the continuum rather than the spectral lines dominates the spectrum: this impression is incorrect for coronal abundances because free–bound emission (which is abundance-dependent) rather than free–free emission (which is not) dominates the continuum. Figure 5 presents the relative contribution of spectral lines to the total flux in the two GOES XRS channels for the assumptions of coronal (solid lines) and photospheric (dashed lines) abundances (cf., Figure 5 of TSC). For photospheric abundances the lines produce less than 20% of the X-ray flux above 20 MK in either GOES channel, but for coronal abundances the 0.5–4 Å channel can have over 30% of its flux above 20 MK due to lines. This is almost entirely contributed by the FeXXV/FeXX complex at 1.85 Å close to the peak in the response of the 0.5–4 Å channel. We note that Phillips (2004) has recently discussed the use of this line complex in conjunction with adjacent continuum to investigate the Fe abundance of flares.

It is also useful to consider the energy ranges of the photons that contribute to the GOES soft X-ray fluxes. The nominal wavelength ranges of 0.5–4 and 1–8 Å correspond roughly to 3–25 and 1.5–12 keV, but, e.g., a temperature of 10 MK corresponds to a photon energy of order 1 keV, and such a spectrum has essentially no photons above a few keV (e.g., see Figure 2), so the upper energy limits quoted above are usually misleading. In Figure 6 we plot the mean photon energy (i.e., averaged using the product of the appropriate transfer function with a model spectrum) and the $\pm 1\sigma$ energy limits (i.e., the energy range that produces the central 68% of the total contribution to the flux) for each of the GOES XRS channels as a function of temperature, derived using the CHIANTI 4.2 coronal and photospheric abundance models. Below 20 MK the two GOES XRS channels are dominated by quite different typical photon energies (the contributing energy

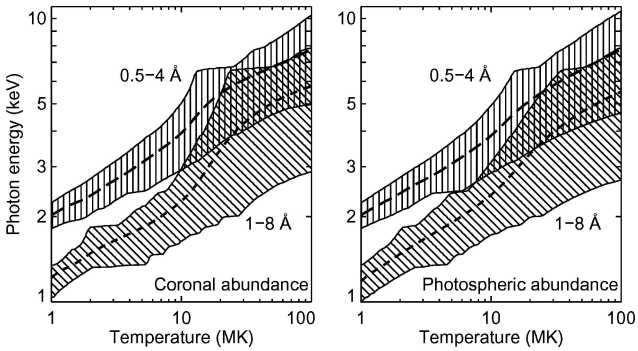


*Figure 6.* Plots of the photon energy ranges contributing to the GOES X-ray responses in each channel as a function of temperature for coronal abundances (*left panel*) and photospheric abundances (*right panel*). The shaded regions indicate the $\pm 1\sigma$ limits of the photon energies contributing to the 0.5–4 Å channel (*vertically shaded region*) and the 1–8 Å channel (*obliquely shaded region*). The *dashed lines* show the mean photon energy contributing to each channel: the mean energy is the photon energy weighted by the product of the spectrum and the appropriate transfer function. The limits of the contributing energy range are defined to be the 16 and 84% levels in the cumulative contribution function. The plot shows results for the GOES 10 detectors.

ranges are separated), with the shorter-wavelength channel seeing more energetic photons as expected, but above 20 MK the model spectra tend to be dominated by emission in the 1–2 Å (6–12 keV) range that contributes to both XRS channels and this reduces the ratio of the mean photon energies contributing to the two channels. The energy range of the photons contributing most to the GOES XRS response is typically about 4 keV in both channels at higher temperatures. The results are very similar for both coronal and photospheric abundances, but there is a small difference in the width of the energy range contributing to the 0.5–4 Å channel at higher temperatures, where the narrow Fe emission feature at 1.85 Å is four times brighter in the coronal abundance spectrum than in the photospheric abundance spectrum and is responsible for a smaller effective width.

## 4. GOES XRS Temperature and Emission Measure Response

We follow the scheme introduced by TSC for deriving the temperature, $T$, and volume emission measure, $EM = N_{\rm e} N_{\rm H} V$, where $N_e$ is the electron density, $N_H$ the proton density and $V$ the volume of the (assumed homogeneous and isothermal) source, from the reported X-ray fluxes $B_4$ (0.5–4 Å channel) and $B_8$ (1–8 Å channel). Since the ratio of the levels in the two channels $R = B_4/B_8$ is a monotonic function of temperature over the range 1–100 MK, it can be inverted to determine the temperature. Once the temperature is known, the emission measure is derived from the reported flux in the 1–8 Å channel using a temperature-dependent scaling factor. The scaling between $R$ and $T$, and between $B_8(T)$ and $EM$, is determined by

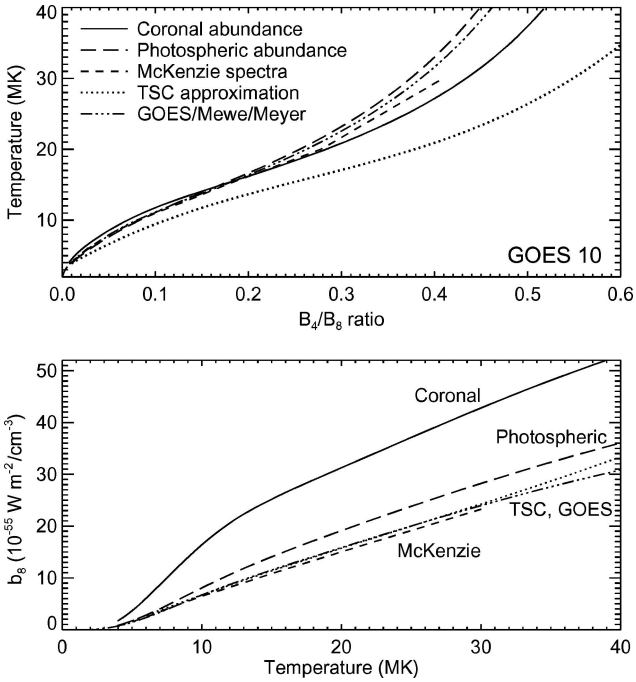


*Figure 7.* Plots of the temperature and emission measure response of the XRS detectors on the GOES 10 satellite for five different sets of models. The *short dashed line* is derived from the McKenzie spectra, while the *dotted line* represents the polynomial approximation derived by TSC for the GOES 1 satellite. The *dash-dot line* labeled "GOES/Mewe/Meyer" is the response for the Mewe spectrum with Meyer (1985) abundances: this is the response used currently in the `goes` widget in SolarSoft. The *long-dashed line* is the response for CHIANTI 4.2 spectra with photospheric abundances, while the *solid line* is for CHIANTI 4.2 spectra with coronal abundances. $B_4/B_8$ is the ratio of the reported X-ray fluxes in the two channels, and $b_8$ is the normalized response of the 1–8 Å channel (flux per unit emission measure). Labels in the lower panel are abbreviated versions of the labels in the upper panel.

calculating GOES XRS responses in the two channels for the model data described in the preceding section. The same approach is employed in the SolarSoft `goes` widget.

The detailed response in terms of fluxes in the two channels varies from one satellite to the next, as described earlier. In Figure 7 we show as an example the response for the GOES 10 XRS detectors. The upper panel of the figure shows the dependence of temperature on the flux ratio for five different responses: the CHIANTI spectrum with coronal abundances (solid line), the CHIANTI spectrum with photospheric abundances (long dashes), the Mewe spectrum with Meyer (1985) abundances used in `goes` in SolarSoft (dash-dots), the original McKenzie spectra used by TSC (short dashes), and the TSC polynomial approximation (dotted line). The temperature response is very similar for the three curves in which

low-FIP abundances are at photospheric levels (CHIANTI/photospheric, Mewe, McKenzie). As noted in the previous section, at higher temperatures the coronal abundance curve produces cooler temperatures for a given $B_4/B_8$ flux ratio due to the shift in the location of the peak wavelength of the continuum emission.

The TSC polynomial approximation does not resemble any of the other curves for GOES 10. This will be the case when applying the original TSC polynomial approximation to data from any satellite after GOES 3, since the TSC formalism was based on a definition of the $\bar{G}_4$ coefficient that was altered starting with GOES 4 (as can be seen in Table I). The effect of that rescaling is to cause a given detected ion-chamber current in the short-wavelength channel of GOES 4–12 to be reported as a smaller soft X-ray flux than if it had been measured by GOES 1–3. A better agreement with the TSC approximation is obtained if the reported 0.5–4 Å fluxes are multiplied by an empirical factor of 1.631/1.16 (Table I) before application of the formalism. For GOES 1–3 we find that the TSC polynomial approximation is indeed close to the responses to photospheric-abundance CHIANTI models at temperatures below 15 MK.

The lower panel of Figure 7 shows the relationship between the 1–8 Å response per unit emission measure, $b_8 = (10^{55}\ \mathrm{cm}^{-3}/EM)\ B_8$, and the temperature. The Mewe, McKenzie and TSC polynomial approximation all have a very similar response, being quite close to linear in temperature as in Figure 4 of TSC. The CHIANTI/photospheric curve shows a slightly larger response, while the CHIANTI/coronal response is substantially larger and has a noticeably different shape, with a steeper slope below 10 MK than above. The impact of the larger response to the CHIANTI coronal spectrum is that a smaller (hydrogen) emission measure is needed to produce a given reported GOES XRS flux value compared with the other spectral models considered.

For completeness and to demonstrate the quantitative nature of the differences in response, we have determined polynomial approximations to the response curves for the CHIANTI model spectra demonstrated in Figure 7. Coefficients for each satellite up to GOES 12, for the cases of both coronal and photospheric abundances, are given in Tables II and III in the appendix, valid in the temperature range from 5 to 30 MK that encompasses most flare emissions detected by GOES. These tables, particularly Table III, show that the original TSC approximation is very similar to our fit with CHIANTI and photospheric abundances for GOES 1–3, particularly for the temperature dependence, but that the parameters differ considerably for GOES 4 and later for the reasons discussed earlier.

To demonstrate the impact of the differences in the responses, Figure 8 compares the temperature and emission measure for a flare on 11 June 1998 derived using the CHIANTI/coronal response (solid lines), CHIANTI/photospheric response (dashed lines), the Mewe/Meyer response (dot-dash lines; obtained from the `goes` program in SolarSoft), and the TSC polynomial approximations. At the temperature peak of the flare during the rise phase of the X-ray flux, the two CHIANTI curves produce the same temperature: this is because the corresponding curves in the top

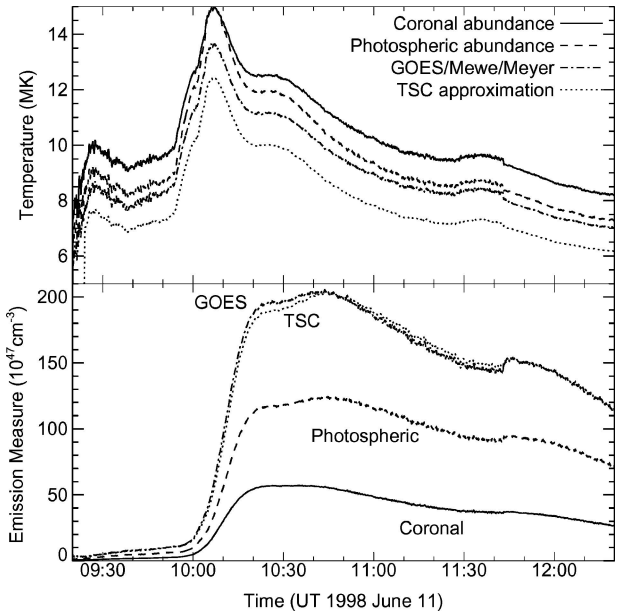


*Figure 8.* Comparison of the temperature (*upper panel*) and emission measure (*lower panel*) derived from GOES soft X-ray data for a flare on 11 June 1998. The four curves are the CHIANTI model with coronal abundances (*solid line*), the CHIANTI model with photospheric abundances (*dashed line*), the Mewe model with Meyer abundances as used in the `goes` widget in SolarSoft (*dot-dashed line*), and the TSC polynomial approximation (*dotted line*). The data (and the responses used) are from the GOES 8 detectors.

panel of Figure 7 cross at 15 MK. The other two responses give consistently lower temperatures, by about 1 MK for the Mewe/Meyer response and 2 MK for the TSC approximations. At lower temperatures the CHIANTI/photospheric values are also about 1 MK below the coronal abundance temperatures.

The higher temperatures found with coronal abundances in this event compound the fact that the coronal abundance response in the lower energy channel $b_8$ is larger than the corresponding photospheric abundance response and the fact that the higher temperature makes $b_8$ larger as well (Figure 7, lower panel). This compound effect leads to emission measures that differ by more than the difference between the coronal and photospheric abundance curves in the lower panel of Figure 7 would suggest, as shown in the lower panel of Figure 8. The Mewe/Meyer and TSC responses give very similar results, but the CHIANTI/photospheric emission measure is about 40% lower and the CHIANTI/coronal emission measure is about half of the photospheric emission measure. Thus, in this event, the assumption of coronal abundances together with the use of modern spectral models leads to emission measures that are a factor of order 4 smaller than current models predict in the case of $<15$ MK flares. At the peak of the flare the total thermal energy of the soft X-ray plasma implied by the Mewe/Meyer response is three times the total

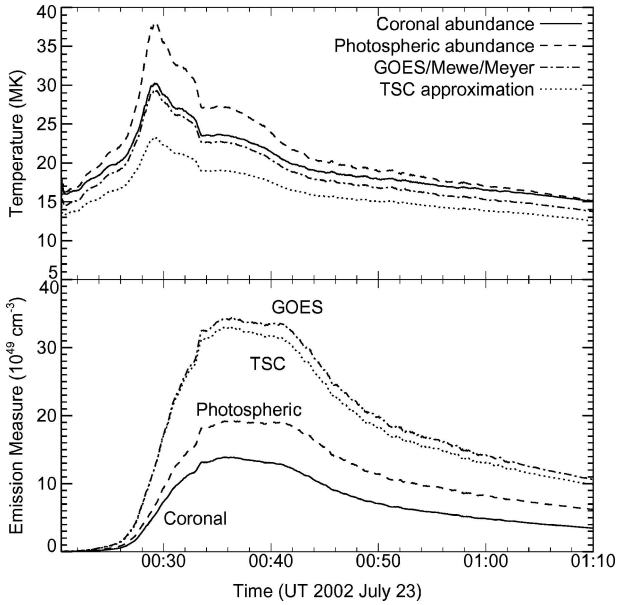


*Figure 9.* Comparison of the temperature (*upper panel*) and emission measure (*lower panel*) derived from GOES soft X-ray data for a flare on 23 July 2002, in the same format as Figure 8. The data (and the responses used) are from the GOES 8 detectors.

energy derived from the CHIANTI coronal-abundance response, and about 50% larger than for the CHIANTI photospheric-abundance response.

Note, however, that at temperatures above 15 MK the opposite effect occurs: for a given ratio of the fluxes in the two channels a smaller temperature will be deduced for coronal abundance than for photospheric abundance, and this will lead to a smaller difference in the derived emission measure. We illustrate this in Figure 9 with the well-known flare of 23 July 2002, which produced much hotter soft X-rays than the previous example. The peak temperature in this event reached about 30 MK, and at these hotter temperatures the photospheric abundance response yields higher temperature determinations than does the coronal abundance response. The resulting derived emission measures show a difference of less than a factor of 2 between the coronal and photospheric abundance CHIANTI models, but again both are much smaller than the older responses would suggest.

## 5. Implementation

The GOES XRS responses calculated using CHIANTI models and both coronal and photospheric abundances for each satellite will be made available through the SolarSoft `goes` package via a routine `goes_chianti_tem` that converts GOES

XRS fluxes in the two channels into a temperature and emission measure under the isothermal assumption. The `goes` widget widely used in SolarSoft to retrieve GOES data and to carry out the conversion to temperature and emission measure will employ this routine and have options added to allow the selection of photospheric or coronal abundances in carrying out the conversion. The "hybrid abundance" (Fludra and Schmelz, 1999) case will lie somewhere between the photospheric and coronal values. The actual coefficients used to do the conversion are contained in routines called `goes_get_chianti_temp` and `goes_get_chianti_em`, while the GOES XRS transfer functions can be found in the routine `goes_transfer.pro`.

## 6. Conclusions

We have investigated the temperature response of the soft X-ray flux measurements from NOAA's GOES series of satellites using modern CHIANTI spectral models with Mazzotta *et al.* (1998) ionization equilibria. We have used model spectra for a range of appropriate temperatures with both coronal and photospheric abundances to determine the response of the GOES XRS detectors as a function of temperature, and these responses may be used to determine temperatures and emission measures under the isothermal assumption. Although the detectors on the individual GOES satellites are quite similar, their data are calibrated in a satellite-dependent fashion and consequently the responses differ from one satellite to another.

An important and perhaps surprising result of this study is that the derived temperature and emission measure depend strongly on the assumed abundances even at high temperatures where continuum rather than spectral lines dominate the Sun's X-ray spectrum. For the currently accepted set of coronal abundances, most of the continuum is due to free–bound emission processes, not free–free emission, and thus is abundance-dependent. We find significant differences between modern calculations of the temperature response of the detectors and the versions currently in use: for a typical flare, emission measures can be up to a factor of 4 smaller than the current software suggests. Derived temperatures are similar for both photospheric and coronal abundances for cool flares (e.g., 15 MK), but for hot flares (e.g., 35 MK) coronal abundances can lead to significantly ($\sim$25%) lower temperatures being derived.

## Acknowledgements

At the University of Maryland this research was supported by NSF grant ATM 02-33907 and NASA grants NAG 5-11872, NAG 5-12860 and NAG 5-10175. We thank Dr. Rodney Viereck of NOAA for supplying the calibration data for the GOES 12 detectors, Brian Dennis, Ken Phillips and Enrico Landi for discussions

and encouragement, Hugh Hudson and Jim McTiernan for advice, Enrico Landi for supplying a model CHIANTI 5.0 spectrum in advance of release for comparison, and the referee Howard Garcia for valuable comments on the manuscript.

## Appendix

As described by TSC and Garcia (1994), the GOES soft X-ray detectors respond to the incident X-ray flux by producing a current. The measured currents are converted to the reported X-ray flux values by dividing the currents by the parameters $\bar{G}_4$ (0.5–4 Å) and $\bar{G}_8$ (1–8 Å) that nominally represent wavelength-averaged transfer functions, i.e., averages over the transfer functions shown in Figure 1. (In practice, the current data are actually telemetered to the ground as voltages that are proportional to the currents and the voltages are converted to fluxes in a single operation: see Garcia (1994)). The following table shows the values currently in use, as well as the nominal operational period for each spacecraft and the period for which we can find data available at the National Geophysical Data Center and/or the Solar Data Analysis Center. The value for $\bar{G}_8$ shown for GOES 6 is the value that applies after 28 June 1993; prior to that date the value $4.43 \times 10^{-6}$ was used for the conversion of current to flux. Note that for their calculations for GOES 1 TSC used values slightly smaller than shown in the table for both $\bar{G}_4$ and $\bar{G}_8$; their values of $1.16 \times 10^{-5}$ and $3.5 \times 10^{-6}$, respectively, differ from the official values by some 10–15%.

TABLE I

$\bar{G}$ normalization coefficients for converting detector currents to X-ray fluxes, as well as the nominal operational period for each spacecraft and the period for which we can find data available at the National Geophysical Data Center and/or the Solar Data Analysis Center.

| Satellite | Operational | XRS data available | $\bar{G}_4$ (A/W m$^{-2}$) | $\bar{G}_8$ (A/W m$^{-2}$) |
|---|---|---|---|---|
| GOES 1 | 1975/10/16–1985/03/07 | 1976/01–1978/05 | $1.27 \times 10^{-5}$ | $4.09 \times 10^{-6}$ |
| GOES 2 | 1977/06/16–1993 | 1977/08–1983/05 | $1.25 \times 10^{-5}$ | $3.98 \times 10^{-6}$ |
| GOES 3 | 1978/06/16–1993 | 1978/07–1980/08 | $1.25 \times 10^{-5}$ | $3.98 \times 10^{-6}$ |
| GOES 4 | 1980/09/09–1988/11/22 | | $1.73 \times 10^{-5}$ | $4.56 \times 10^{-6}$ |
| GOES 5 | 1981/05/22–1990/07/18 | 1983/01–1987/02 | $1.74 \times 10^{-5}$ | $4.84 \times 10^{-6}$ |
| GOES 6 | 1983/04/28– | 1983/05–1994/08/18 | $1.74 \times 10^{-5}$ | $5.32 \times 10^{-6}$ |
| GOES 7 | 1987/02/26–1996/08/03 | 1987/03–1996/08/03 | $1.68 \times 10^{-5}$ | $4.48 \times 10^{-6}$ |
| GOES 8 | 1994/04/13–2004/05/05 | 1996/03/21–2003/06/18 | $1.580 \times 10^{-5}$ | $4.165 \times 10^{-6}$ |
| GOES 9 | 1995/05/23– | 1996/03/20–1998/09/08 | $1.607 \times 10^{-5}$ | $3.990 \times 10^{-6}$ |
| GOES 10 | 1997/04/25– | 1998/07/10– | $1.631 \times 10^{-5}$ | $3.824 \times 10^{-6}$ |
| GOES 11 | 2000/05/03– | Backup | | |
| GOES 12 | 2001/07/23– | 2002/12/13– | $1.595 \times 10^{-5}$ | $4.090 \times 10^{-6}$ |

TABLE II

Coefficients for polynomial approximations to GOES temperature response: coronal abundances.

| Satellite | $A(0)$ | $A(1)$ | $A(2)$ | $A(3)$ | $B(0)$ | $B(1)$ | $B(2)$ | $B(3)$ |
|---|---|---|---|---|---|---|---|---|
| TSC | 3.15 | 77.2 | −164.0 | 205.0 | −3.86 | 1.17 | −0.0131 | 0.000178 |
| GOES 1 | 3.74 | 77.5 | −158.0 | 180.3 | −12.80 | 3.88 | −0.1020 | 0.001210 |
| GOES 2 | 3.74 | 78.3 | −161.7 | 186.6 | −13.15 | 3.99 | −0.1048 | 0.001243 |
| GOES 3 | 3.74 | 78.3 | −161.7 | 186.6 | −13.15 | 3.99 | −0.1048 | 0.001243 |
| GOES 4 | 3.74 | 94.6 | −235.9 | 328.9 | −11.48 | 3.48 | −0.0915 | 0.001085 |
| GOES 5 | 3.74 | 89.7 | −211.8 | 279.8 | −10.81 | 3.28 | −0.0862 | 0.001022 |
| GOES 6 | 3.83 | 86.2 | −193.3 | 242.1 | −10.25 | 3.12 | −0.0836 | 0.000997 |
| GOES 7 | 3.68 | 101.2 | −271.3 | 409.3 | −11.87 | 3.54 | −0.0882 | 0.001027 |
| GOES 8 | 4.02 | 100.3 | −258.1 | 366.5 | −12.56 | 3.87 | −0.1077 | 0.001298 |
| GOES 9 | 3.97 | 100.8 | −260.7 | 373.1 | −12.63 | 3.91 | −0.1097 | 0.001326 |
| GOES 10 | 3.81 | 101.5 | −270.7 | 404.6 | −12.03 | 3.61 | −0.0928 | 0.001091 |
| GOES 12 | 3.90 | 101.2 | −266.4 | 390.2 | −12.31 | 3.75 | −0.1003 | 0.001195 |

TABLE III

Coefficients for polynomial approximations to GOES temperature response: photospheric abundances.

| Satellite | $A(0)$ | $A(1)$ | $A(2)$ | $A(3)$ | $B(0)$ | $B(1)$ | $B(2)$ | $B(3)$ |
|---|---|---|---|---|---|---|---|---|
| TSC | 3.15 | 77.2 | −164.0 | 205.0 | −3.86 | 1.17 | −0.0131 | 0.000178 |
| GOES 1 | 3.06 | 75.3 | −145.9 | 210.9 | −5.70 | 1.59 | −0.0169 | 0.000110 |
| GOES 2 | 3.06 | 76.2 | −149.3 | 218.3 | −5.85 | 1.63 | −0.0174 | 0.000113 |
| GOES 3 | 3.06 | 76.2 | −149.3 | 218.3 | −5.85 | 1.63 | −0.0174 | 0.000113 |
| GOES 4 | 3.06 | 92.0 | −217.9 | 384.7 | −5.11 | 1.42 | −0.0152 | 0.000099 |
| GOES 5 | 3.06 | 87.2 | −195.6 | 327.4 | −4.81 | 1.34 | −0.0143 | 0.000093 |
| GOES 6 | 3.15 | 84.1 | −178.9 | 283.3 | −4.56 | 1.28 | −0.0145 | 0.000101 |
| GOES 7 | 2.98 | 98.8 | −250.6 | 478.2 | −5.33 | 1.45 | −0.0129 | 0.000062 |
| GOES 8 | 3.36 | 98.6 | −242.0 | 434.0 | −5.54 | 1.58 | −0.0201 | 0.000158 |
| GOES 9 | 3.31 | 98.6 | −242.7 | 439.2 | −5.56 | 1.59 | −0.0208 | 0.000168 |
| GOES 10 | 3.15 | 99.2 | −250.9 | 473.8 | −5.37 | 1.48 | −0.0145 | 0.000084 |
| GOES 12 | 3.24 | 99.2 | −247.9 | 458.8 | −5.47 | 1.53 | −0.0173 | 0.000121 |

TSC derived polynomial approximations that allow one to derive the temperature, $T$, and volume emission measure, $EM = N_e N_H V$, from the ratio $R = B_4/B_8$ of the reported X-ray fluxes $B_4$ (0.5–4 Å) and $B_8$ (1–8 Å), and the value of $B_8$ as follows: the temperature is obtained from

$$T(R) = A(0) + A(1)R + A(2)R^2 + A(3)R^3 \quad (1)$$

and once the temperature is known the emission measure is derived from $EM = 10^{55}\, B_8/b_8(T)\,\mathrm{cm}^{-3}$ where $B_8$ is the 1–8 Å flux in the standard GOES unit of W m$^{-2}$ and

$$b_8(T) = B(0) + B(1)T + B(2)T^2 + B(3)T^3 \tag{2}$$

is the normalized response.

We have derived such polynomial approximations for all GOES satellites using CHIANTI spectral models as discussed earlier. The next two tables present the $A(0-3)$ and $B(0-3)$ coefficients for each satellite, as well as the original TSC values. The next table presents the coefficients under the assumption of coronal abundances, while the last table presents the coefficients for photospheric abundances. They result from fitting curves such as those shown in Figure 7 ($T$ versus $R$ and $b_8$ versus $T$ for GOES 10) over the temperature range 4–40 MK. The fits work well in the range 5–40 MK: temperatures are always correct to within 4% (coronal abundances) or 2% (photospheric abundances) and emission measures are correct to within 9% (coronal) or 8% (photospheric) across this range, with the errors largest at low temperatures where the $B_4/B_8$ ratio is very small. In the range 10–40 MK which is appropriate for most solar flares, the errors in the emission measure are always less than 4%. However, the tabulated data used in the IDL routines available through SolarSoft are more accurate than these polynomial approximations and should be used whenever possible.

## References


Aschwanden, M. J. and Alexander, D.: 2001, *Solar Phys.* **204**, 91.

Bornmann, P. L.: 1990, *Astrophys. J.* **356**, 733.

Brown, G. V., Beiersdorfer, P., Liedahl, D. A., Widmann, K., Kahn, S. M., and Clothiaux, E. J.: 2002, *Astrophys. J. Suppl.* **140**, 589.

Dere, K. P., Landi, E., Mason, H. E., Monsignori Fossi, B. C., and Young, P. R.: 1997, *Astron. Astrophys. Suppl. Ser.* **125**, 149.

Feldman, U.: 1992, *Physica Scripta* **46**, 202.

Feldman, U. and Laming, J. M.: 2000, *Physica Scripta* **61**, 222.

Feldman, U. and Widing, K. G.: 2003, *Space Sci Rev.* **107**, 665.

Fludra, A. and Schmelz, J. T.: 1999, *Astron. Astrophys.* **348**, 286.

Freeland, S. L. and Handy, B. N.: 1998, *Solar Phys.* **182**, 497.

Garcia, H. A.: 1994, *Solar Phys.* **154**, 275.

Garcia, H. A.: 2004, *Space Weather* **2**, S06003.

Gu, M. F., Kahn, S. M., Savin, D. W., Behar, E., Beiersdorfer, P., Brown, G. V., Liedahl, D. A., and Reed, K. J.: 2001, *Astrophys. J.* **563**, 462.

Jordan, C.: 1970, *Monthly Notices Royal Astron. Soc.* **148**, 17.

Landi, E., Feldman, U., and Dere, K. P.: 2002, *Astrophys. J. Suppl.* **139**, 281.

Landi, E., Landini, M., Dere, K. P., Young, P. R., and Mason, H.E.: 1999, *Astron. Astrophys. Suppl. Ser.* **135**, 339.

Liedahl, D. A., Osterheld, A. L., and Goldstein, W. H.: 1995, *Astrophys. J. (Lett.)* **438**, L115.

Mazzotta, P., Mazzitelli, G., Colafrancesco, S., and Vittorio, N.: 1998, *Astron. Astrophys. Suppl. Ser.* **133**, 403.
Mewe, R., Gronenschild, E. H. B. M., and van den Oord, G. H. J.: 1985, *Astrophys. J. Suppl.* **62**, 197.
Meyer, J.-P.: 1985, *Astrophys. J. Suppl.* **57**, 173.
Phillips, K. J. H.: 2004, *Astrophys. J.* **605**, 921.
Phillips, K. J. H. and Feldman, U.: 1995, *Astron. Astrophys.* **304**, 563.
Raymond, J. C. and Smith, B. W.: 1977, *Astrophys. J. Suppl.* **35**, 419.
Savin, D. W., Beiersdorfer, P., Lopez-Urrutia, J. C., Decaux, V., Gullikson, E. M., Kahn, S.M., Liedahl, D. A., Reed, K. J., and Widmann, K.: 1996, *Astrophys. J. (Lett.)* **470**, L73.
Schmelz, J. T.: 1999, in *ESA SP-446: 8th SOHO Workshop: Plasma Dynamics and Diagnostics in the Solar Transition Region and Corona*, p. 585.
Sylwester, J., Garcia, H. A., and Sylwester, B.: 1995, *Astron. Astrophys.* **293**, 577.
Thomas, R. J., Starr, R., and Crannell, C.-J.: 1985, *Solar Phys.* **95**, 323.
Veronig, A. M., Brown, J. C., Dennis, B. R., Schwartz, R. A., Sui, L., and Tolbert, A. K.: 2005, *Astrophys. J.* **621**, 482.
Walker, Jr., A. B. C., Rugge, H. R., and Weiss, K.: 1974, *Astrophys. J.* **188**, 423.
White, S. M., Thomas, R., Brosius, J. W., and Kundu, M. R.: 2000, *Astrophys. J. (Lett.)* **534**, L203.
Young, P. R., Landi, E., and Thomas, R. J.: 1998, *Astron. Astrophys.* **329**, 291.
Young, P. R., del Zanna, G., Landi, E., Dere, K. P., Mason, H. E., and Landini, M.: 2003, *Astrophys. J. Suppl.* **144**, 135.